High-force NdFeB-based magnetic tweezers device optimized for microrheology experiments

Jun Lin and Megan T. Valentine

Citation: Review of Scientific Instruments **83**, 053905 (2012); doi: 10.1063/1.4719916
View online: http://dx.doi.org/10.1063/1.4719916
View Table of Contents: http://scitation.aip.org/content/aip/journal/rsi/83/5?ver=pdfcov
Published by the AIP Publishing

High-force NdFeB-based magnetic tweezers device optimized for microrheology experiments

Jun Lin[1,2] and Megan T. Valentine[1,a)]
[1]*Department of Mechanical Engineering, University of California, Santa Barbara, California 93106, USA*
[2]*Biomolecular Science and Engineering Program, University of California, Santa Barbara, California 93106, USA*

(Received 11 January 2012; accepted 5 May 2012; published online 24 May 2012)

We present the design, calibration, and testing of a magnetic tweezers device that employs two pairs of permanent neodymium iron boron magnets surrounded by low-carbon steel focusing tips to apply large forces to soft materials for microrheology experiments. Our design enables the application of forces in the range of 1–1800 pN to ~4.5 μm paramagnetic beads using magnet-bead separations in the range of 0.3–20 mm. This allows the use of standard coverslips and sample geometries. A high speed camera, custom LED-based illumination scheme, and mechanically stabilized measurement platform are employed to enable the measurement of materials with viscoelastic moduli as high as ~1 kPa. © *2012 American Institute of Physics*. [http://dx.doi.org/10.1063/1.4719916]

I. INTRODUCTION

A number of active microrheology methods have been developed to determine the viscoelastic properties of soft materials as a function of applied force.[1] Microrheology measurements are particularly useful in determining the spatial distributions of stiffness and/or viscosity in heterogeneous materials, or in determining the moduli of precious samples that cannot be obtained in large quantities.[2] Experimental platforms commonly incorporate an optical microscope to visualize samples and direct the application of force using microscale probes. AFM-based methods can apply large indentation stresses (~0.1–10 kPa) to soft interfaces and provide simultaneous topographical information, but cannot easily probe the 3-dimensional properties of polymer solutions or gels.[3] Optical trapping methods provide nanometer-resolution of probe position and can operate at high frequencies.[4,5] However, optically transparent materials of fairly low index of refraction are required, and since the maximum applied force is typically tens of picoNewtons, use of optical trapping methods has been limited to fairly soft materials (<50 Pa). For both optical traps and AFM, the application of constant force requires computer-controlled feedback control to compensate for instrument compliance.

Magnetic tweezers devices provide a valuable alternative, allowing for the characterization of 3D materials while providing ~nanoNewton forces. However, previous implementations of high-force magnetic tweezers for microrheology have typically relied on the use of electromagnets operating at high current, which can heat samples and exhibit a hysteretic response, or on extremely small distances (~micrometer) between the pole pieces and magnetic beads, or both.[6–8] These constraints can lead to unusual experimental geometries with potential interference to high-resolution microscopy, can create steep force gradients within the image plane, and, in the case of devices in which iron pole pieces are submerged into the sample, can create chemically reactive metal ions. By contrast, neodymium iron boron (NdFeB)-based magnetic tweezers are non-invasive and easily provide constant force to the sample plane without the use of feedback control. Because of these advantages, NdFeB magnets have become a standard technology for single molecule force-spectroscopy where femto- to picoNewton forces are required;[9,10] however, these have thus far found limited utility in meso- to macroscale materials characterization, which typically requires larger forces to achieve measurable deformations.

In this report, we present the design, calibration, and testing of a new magnetic tweezers device that employs two pairs of permanent NdFeB magnets surrounded by low-carbon steel focusing tips to apply large forces to soft materials for microrheology experiments. Our design enables the application of forces in the range of 1–1800 pN to ~4.5 μm paramagnetic beads using standard coverslips and sample geometries. The maximum applied force is roughly an order of magnitude higher than previous designs, making it possible to study materials with viscoelastic moduli as high as ~1 kPa.

II. APPARATUS

A. Overview of instrument design

A simple inverted microscope serves as the basis of our optical design (Fig. 1). A Nikon CFI Plan Fluor 100× oil-immersion objective is mounted onto a Fast PIFOC® Piezo Nanofocusing Drive, with 250 μm travel distance (Physik Instrumente). A turning mirror is placed below the objective to direct the image onto a CMOS camera (Point Grey), which is connected to a computer workstation (Dell) using a Camera Link framegrabber PCI card (National Instruments). The sample is placed on a custom heavy-duty platform to minimize vibrations. A manual *x*-*y* positioning stage (Marzhauser) with excellent mechanical stability is used to scan through the sample during imaging. Above the sample plane, the custom-designed magnet assembly and illumination optics are mounted; both systems are described in detail below.

a)Author to whom correspondence should be addressed. Electronic mail: valentine@engineering.ucsb.edu.

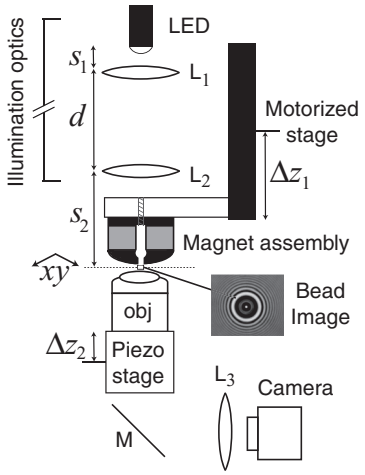

FIG. 1. Schematic of the instrument. The magnet assembly is positioned just above the sample plane (dotted line) and mounted onto a long-distance travel motorized stage, which allows the assembly to be moved a height Δz_1 (typically $\Delta z_1 < 30$ mm) at speeds of up to ~100 mm/s. Above the magnets, the illumination optics consists of the LED housing with built-in collimating lens (L_1), which is placed a distance $s_1 \sim 8$ mm away from the LED array. We defocus this system slightly to ensure a gently divergent beam. A second compound lens (L_2) is placed a distance $d = 820$ mm away. This compound lens consists of a 250-mm focal length lens, followed by a 500-mm focal length lens placed 8 mm apart. The focal length of the compound lens is ~168 mm. The distance between L_2 and the sample plane, s_2 is 220 mm. Below the sample plane, a 100× objective lens, mounted on a precision piezoelectric one-axis translation stage, is used to form an image. A turning mirror M directs the image to the camera, which is formed by L_3, a simple 150-mm relay lens.

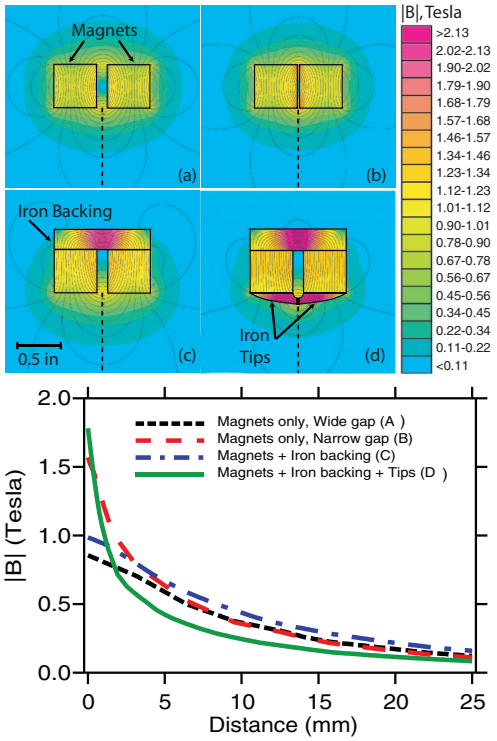

FIG. 2. Results of FEMM 2D simulations. Four magnet assembly designs are tested, as shown in the upper panel, consisting of magnets only (a and b), magnets with an iron backing (c), and magnets with an iron backing and focusing tips (d). The upper panel shows 2D heat maps of the magnetic field amplitudes |B|. The solid lines outline the shapes of the magnets and iron pieces, as indicated. The dotted line indicates the line along which |B| field is calculated as a function of distance, as shown in the lower panel. Simulation D (solid line) provided both the highest magnetic field amplitude, and the steepest field gradient, and thus served as the basis of our physical design.

B. Optimize magnet assembly design for high force applications

Our magnet assembly incorporates two pairs of strong NdFeB magnets (0.5-in. cubes; NS-505050; DuraMag) and iron "pole pieces" to confine and direct the magnetic fields in order to produce the highest possible field gradient at the sample plane. To optimize the design process for the magnet assembly, we employ a widely available finite element (FE) software package (finite element method magnetics (FEMM), using the Newton AC solver with 10^{-8} precision to minimize the angle for any vertex).[11,12] Use of 3D FE packages to calculate magnetic fields has been shown to quantitatively predict field strengths and gradients.[13] Here, we show that simpler simulations, in which the shape, orientation, and materials properties of 2D objects are specified, are also very effective in qualitatively predicting how the addition of high magnetic permeability materials confine and direct the magnetic fields.

To rapidly compare various designs, we compare heat maps of the 2D magnetic field amplitude, as well as the 1D field magnitude as a function of distance away from the magnet assembly along the symmetry axis (Fig. 2). A distance of zero indicates that the assembly is in contact with the sample. Here, we present four examples to demonstrate the utility of this method: (a) magnet pair only, with separation distance of 2.54 mm, (b) magnet pair only, with separation distance of 1 mm, (c) magnet pair with separation distance of 2.54 mm connected with an iron backing, (d) magnet pair with separation distance of 2.54 mm connected with an iron backing and iron-focusing tips with a minimum separation of 1 mm. The upper radius of the focusing tips is determined by the half circle that connects the magnet pair. The lower radius of curvature is ~25 mm.

By comparing (a) and (b) in Fig. 2, we find that reducing the distance between the magnet pairs increases the field amplitude and gradient, with the greatest improvement observed at small distances. Inclusion of iron, a high magnetic permeability material, in a backing (c) provides a modest enhancement in field strength, but does not substantially improve the field gradient. However, the addition of shaped iron tips to direct and focus the fields at the sample plane (d) had a dramatic effect. The tips not only improve field strength, but also increase field gradient, which, in the limit of saturation of the bead magnetic moments, is directly proportional to the force applied to the magnetic beads.

To achieve nanoNewton-scale forces, we implement a modified version of (d), in which two pairs of magnets (each a 0.5-in. cube of N50 NdFeB) are mounted into an aluminum housing that also contains a pair of low-carbon steel (LCS) backing bars ($1.2 \times 0.5 \times 0.25$ in.^{3}) and two LCS-focusing tips (thickness of 0.25 in.) that are press fit between the magnet pairs and extend toward the sample (Fig. 3). Iron and LCS have similar magnetic permeability, but LCS is easier to obtain and machine, so is preferred for this application. A small (~4 mm) hole is bored through the center of the housing to

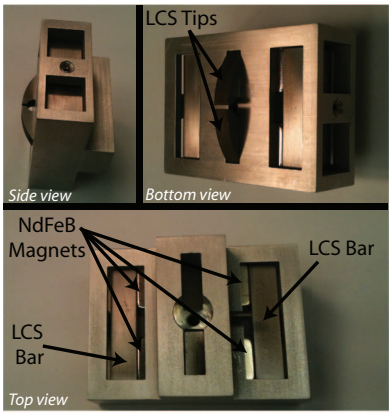

FIG. 3. Images of the completed magnet assembly. An aluminum housing holds four 0.5-in. cube NdFeB N50 magnets between two LCS bars. Below the magnet arrays, two LCS tips are press fit into the housing to direct and focus the magnetic fields.

allow the focused LED light to pass through the LCS tips to illuminate the sample.

C. Optimize for fast force switching without disruption of 3D bead tracking accuracy

Microrheology measurements frequently require fast switching of force amplitudes, either to apply oscillatory stress to a sample, or to apply step stress pulses in a creep measurement protocol.[2] This contrasts the majority of NdFeB-based magnetic tweezers measurements that are performed at fixed force conditions to probe the steady-state behaviors of single-molecules of polymers and motor proteins.[9,10] Fast force switching is easily implemented using electromagnets by the rapid modulation of the driving current. For NdFeB-based magnetic tweezers, force levels are modulated by the physical separation of the magnets and sample. Although the incorporation of a fast linear motor to move the magnets is trivial, the ability to track accurately bead position during the repeated long-distance travel of the magnet array is more challenging. To achieve the accurate bead tracking during fast force switching, our design incorporates a very stable long-distance travel motorized stage, a bright illumination source the intensity of which does not vary as the magnet array moves, and a high-speed data acquisition system.

To ensure mechanical stability, the instrument is mounted onto an air-cushioned optical table. A very stable, long-distance travel motorized stage (Physik Instrumente, M414.1PD) is chosen to achieve high pulling force (200 N) and high velocity (100 mm/s). For a typical microrheology experiment, the magnet array is moved at most 15–20 mm to switch the applied force on or off. At maximum motor travel speed, this transition would take ∼150–200 ms. An internal PID (proportional-integral-derivative) controller, tuned to maximize acceleration, ensures ∼microscale repeatability. The motor is mounted onto a heavy column (Thorlabs, XT95-1000) filled with ∼1 mm steel shot and the sample is mounted onto a custom-built heavy-duty platform to damp vibrations.

To maintain the tracking accuracy, the illumination intensity must be constant over the entire magnet travel distance. To achieve this, we use a very bright LED light source (Roithner, RC-LED-650-02) driven by a stable, current-regulated power supply, and focus the light onto the sample using a custom-built optical collection system. This system must meet two critical demands. First, as much LED light must be collected and focused onto the sample as is possible; this will ensure that images can be collected at high frame rates (>100 frames per second (fps)) without substantial contributions of shot noise. Second, the beam waist must be small enough to pass through the LCS tips, and the focal depth must be large enough to allow the height of the LCS tips to be adjusted without clipping the focused LED beam. To achieve the desired force range for microrheology measurements, the focal depth must be ∼20–30 mm. In practice, this requires the illumination arm to be ∼1 m long (Fig. 1). In our design, we mount the LED and illumination optics onto the same damped column that supports the long-distance travel motorized stage.

To acquire and process data quickly, we choose a high-resolution camera, fast framegrabber, and high-performance computer workstation for real time data analysis. We use a CMOS-based camera (Gazelle, Point Grey) with a 2048 × 1024 array of 5.5 μm square pixels with the maximum frame rate of 280 fps for full frame collection. An 8-tap Camera Link framegrabber card (National Instruments NI PCIe-1433) is used to capture images and relay them to the image processing computer. Images are processed in real time to determine the three-dimensional bead position in each frame using custom image analysis routines written in LabVIEW (National Instruments).[14] To maximize the number of beads that can be simultaneously tracked, we select a Dell workstation with a single-chip quad-core processor (Intel® Xeon® Processor X5687) with 3.60 GHz clock speed, 6.4 GT/s quickpath interconnect, and a 12 MB smart cache.

We have found that a fast, "large" cache memory is particularly important for the rapid processing of the large image stacks required for 3D tracking of beads in these experiments. This tracking is achieved using a FFT-based particle tracking algorithm implemented in LabVIEW (National Instruments).[14] An autocorrelation of each Fourier image is used to determine the *xy* centroid position of the bead, with a typical lateral resolution of ∼5 nm. Axial position detection is achieved using semi-coherent, parallel illumination to generate a diffraction ring pattern that depends sensitively on the distance of the particle from the focal plane. Each image is compared to a look-up table of previously acquired calibration images, and interpolation is used to find the best *z* coordinate, with an axial resolution of ∼10 nm. Because gel microrheology measurements often involve large particle displacements, this calibration image stack typically consists of ∼300 images, where the total calibrated distance is ∼30 μm with 10 reference images collected per μm in the image plane.

With this data acquisition system, we are able to track ∼6 beads at 280 fps in real time using the full 2048 × 1024 pixel array. Tracking more beads is possible, but requires a reduction in image size by cropping or binning, decreased frame rate, use of a smaller calibrated image stack size, and/or the elimination of other computer demands (such as real time data display).

III. EXPERIMENT

A. Pico- to nanoNewton scale forces are achieved

Two complementary approaches are used to calibrate the forces applied to 4.5 μm magnetic beads (Dynabeads, Invitrogen) as a function of magnet separation distance. For low forces below ~60 pN, we track the Brownian motion of a magnetic bead that is tethered to the coverslip by a single DNA molecule. In this geometry, the DNA is stretched as the bead is pulled upwards toward the magnet, thus acts as a simple inverted pendulum.[15] The lateral spring constant is given by the ratio of the vertical force to the DNA length. This spring constant is determined by fitting the measured power spectrum in position to that predicted from an overdamped Langevin equation of motion for a particle in a harmonic potential.[9] This procedure is repeated at each desired magnet position until the force-separation calibration curve is obtained (Fig. 4, triangles).

For forces greater than ~60 pN, DNA stretching behavior no longer provides a useful calibration standard.[16] Instead, we measure the velocity at which single 4.5 μm diameter beads move through a pure glycerol solution and relate this velocity to the force using Stokes law (Fig. 4, circles). We independently determine the glycerol viscosity to be ~1.15 Pa s using a strain-controlled rheometer (ARES-LS, TA Instruments) with a cone-plate tool geometry (50 mm diameter, 0.04 radians cone angle, and 0.045 mm gap) at ~19 °C and a strain rate of 1 revolutions/s. Using our fast CCD camera, we can reliably measure velocities over the range of ~0.005–300 μm/s. In the range of 1–60 pN, for which calibration data using DNA stretching are also available, we find excellent agreement between the two methods (Fig. 4, inset).

Thus, for the magnetic assembly described here, we easily achieve >3 orders of magnitude in the dynamic force range. To complete this calibration, we have used fairly large incremental displacements (~0.5–1 mm), but the motorized stage is accurate in positioning to ~1 μm, so finer calibrations are possible once the working range for a particular experiment is established. For fixed bead types (such as the 4.5-μm Dynabeads (Invitrogen) used here), the application of smaller forces is possible by further increasing the bead-magnet separation distance,[17] but these calibrations are difficult and this force range is not useful to our gel microrheology experiments, so it is not explored here. The application of larger forces is in principle possible, but would require redesign of the magnet assembly, and may require the use of materials with higher magnetic permeability to focus further the magnetic fields.

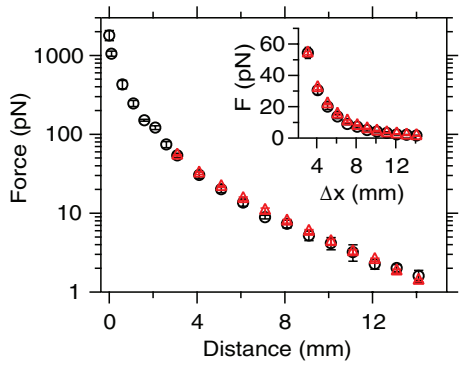

FIG. 4. Calibration curve for force, F, versus distance, Δx, between the magnet assembly and the sample plane. Data represented by circles were obtained by measuring the velocity at which 4.5-μm diameter beads moved through a glycerol solution of known viscosity. Data represented by the triangles were obtained by measuring the stretching of single DNA strands of known length under force. The main figure shows the data plotted on a log-lin plot to display the over three orders of magnitude in applied force that can be achieved with this technique. The inset shows the overlay of data obtained by the two calibration methods on a lin-lin plot. At each displacement, the two force estimates agree within error, given here by the SEM value determined from N repeated measurements ($N = 6$–10).

B. Application to polyacrylamide gel elasticity measurement

To demonstrate the utility of this instrument in measuring the elastic properties of polymeric materials, we prepare crosslinked polyacrylamide gels using 3% acrylamide and 0.06% bis-acrylamide. To initiate polymerization, ammonium persulfate and TEMED were added to the final concentrations of 0.05% and 0.15%, respectively. Bulk rheology measurements have shown these gels to have a shear modulus of ~230 Pa.[18,19] All reagents are mixed with 4.5-μm magnetic beads and immediately loaded into thin capillary tubes (0.1 × 1 × 50 mm^3) to allow the gels to solidify *in situ*. Prior to gel loading, the capillary tubes are cleaned by rinsing with 1 M sodium hydroxide, then pre-coated with reference beads to enable the subtraction of mechanical/thermal drift, or vibration of the sample and/or stage from the real motion of the embedded magnetic particles.[20] To avoid boundary effects arising from the glass/gel interface, we track particles that are at least 25 μm away from the glass surface.

Using our high-force magnetic tweezers, we apply a series of force pulses that ramp up to a maximum force of 1.8 nN, then back down to zero (Fig. 5). Each pulse provides a constant force for approximately 15 s, followed by a period of similar duration at no force. We track bead position in three dimensions as a function of time, and find the gels to respond as elastic solids, with no obvious time-dependent reorganization and no hysteresis. At each force, we calculate gel stiffness by dividing the applied force by the observed average bead displacement (Fig. 6). To emphasize the microscale nature

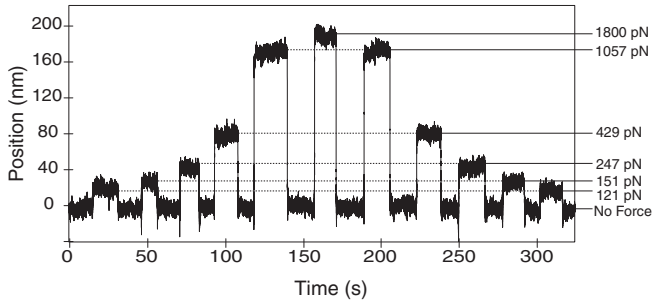

FIG. 5. (Two column figure) Representative trace of bead position as a function of time, as the particle is subjected to a series of force pulses. The force amplitude for each pulse is shown at the right of the graph. Bead position is constant under constant force, consistent with elastic solid behavior, and no obvious hysteresis is observed.

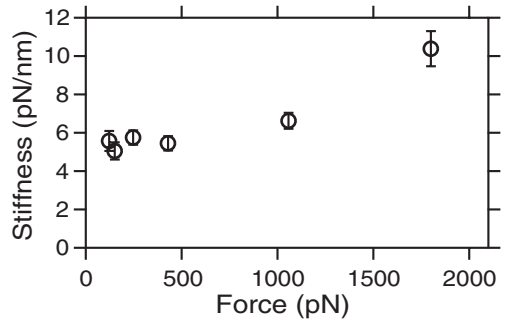

FIG. 6. Polyacrylamide gel stiffness as a function of applied force. Each data point is the average of $N = 11$–20 individual experiments; error bars are given by SEM. For small forces (<500 pN), we find linear elastic behavior. For larger forces, stress-stiffening is observed.

of this measurement, we report our results in terms of stiffness k, rather than modulus G', a macroscopic material property. We find that k is independent of applied force for forces <500 pN. In the case of an infinite homogeneous viscoelastic medium, $G' = k/6\pi a$, where a is the bead radius.[21] For the polyacrylamide gels, we anticipate that the bead diameter is much larger than any structural length scale, and thus bead displacement can be converted into a gel modulus.[22] Under this assumption, we would estimate $G' \sim 130$ Pa at low force, which agrees with the reported macroscopic value within a factor of two.[18,19]

For larger forces, stress stiffening is observed. This contrasts previous studies of the strain-dependence of polyacrylamide gel elasticity using macroscopic rheology, which have shown linear behavior for strains of order unity.[23,24] However, it is in qualitative agreement with the results of micropipette aspiration experiments that showed stress-stiffening for similar polyacrylamide gels under high applied pressures.[25] These data suggest that polyacrylamide gels can stiffen substantially when subjected to localized tension and the extent of stiffening may be sensitive to the geometry by which the load is applied. This is of particular importance to cell traction force measurements in which the deformation of polyacrylamide gels is directly interpreted in terms of local cell stress assuming a linear model of gel elasticity.[26–28]

IV. CONCLUSIONS

We have presented the design, calibration, and testing of a NdFeB-based magnetic tweezers device that can apply large forces in the range of 1–1800 pN to ~4.5 μm paramagnetic beads (with 20% iron content) using standard coverslips and sample geometries. When used in combination with a high speed camera, custom LED-based illumination, and a mechanically stabilized measurement platform, it is possible to measure materials with viscoelastic moduli up to ~1 kPa. We have previously shown that it is possible to increase the force range ~50-fold through the use of larger magnetic beads with diameter of 45 μm and iron content of 4.9%.[29] In cases where such larger beads can be utilized, we would predict maximum forces in the range of 100 nN, a force range that would enable the characterization of materials with elastic moduli of up to ~50 kPa. This is a substantial improvement over existing microrheology methods, and will enable measurements of a broad class of microstructured polymeric materials.

ACKNOWLEDGMENTS

Authors thank Bugra Kaytanli, Yali Yang, Omar Saleh, and the Saleh Laboratory for technical assistance and many helpful discussions. We are grateful for the support of a Burroughs Wellcome Fund Career Award at the Scientific Interface (to M.T.V.) and a Hellman Family Faculty Fellowship Award (to M.T.V.). Viscosity measurements were performed in the MRL UCSB Polymer Facility, supported by National Science Foundation (NSF) (Grant No. DMR-1121053).

[1] L. C. Wilson and W. C. K. Poon, Phys. Chem. Chem. Phys. **13**, 10617–10630 (2011).
[2] M. L. Gardel, M. T. Valentine, and D. A. Weitz, in *Microscale Diagnostic Techniques*, edited by K. Breuer (Springer, 2005).
[3] D. Kirmizis and S. Logothetidis, Int. J. Nanomedicine **5**, 137–145 (2010), http://www.ncbi.nlm.nih.gov/pmc/articles/PMC2865008/pdf/ijn-5-137.pdf.
[4] M. T. Valentine, N. R. Guydosh, B. Gutierrez-Medina, A. N. Fehr, J. O. Andreasson, and S. M. Block, Opt. Lett. **33**(6), 599–601 (2008).
[5] D. Preece, R. Warren, R. M. L. Evans, G. M. Gibson, M. J. Padgett, J. M. Cooper, and M. Tassieri, J. Opt. **13**(4), 044022 (2011).
[6] P. Kollmannsberger and B. Fabry, Rev. Sci. Instrum. **78**(11), 114301 (2007).
[7] A. H. B. de Vries, B. E. Krenn, R. van Driel, and J. S. Kanger, Biophys. J. **88**(3), 2137–2144 (2005).
[8] A. R. Bausch, W. Möller, and E. Sackmann, Biophys. J. **76**(1), 573–579 (1999).
[9] K. C. Neuman and A. Nagy, Nat. Methods **5**(6), 491–505 (2008).
[10] M. Manosas, A. Meglio, M. M. Spiering, F. Ding, S. J. Benkovic, F. X. Barre, O. A. Saleh, J. F. Allemand, D. Bensimon, and V. Croquette, Methods Enzymol. **475**, 297–320 (2010).
[11] N. Pamme, Lab. Chip. **6**(1), 24–38 (2006).
[12] D. C. Meeker, Finite Element Method Magnetics (FEMM Version 4.2, 01 Oct. 2011 Build); see http://www.femm.info/.
[13] J. Lipfert, X. Hao, and N. H. Dekker, Biophys. J. **96**(12), 5040–5049 (2009).
[14] C. Gosse and V. Croquette, Biophys. J. **82**(6), 3314–3329 (2002).
[15] T. R. Strick, J. F. Allemand, D. Bensimon, A. Bensimon, and V. Croquette, Science **271**, 1835–1837 (1996).
[16] S. B. Smith, Y. Cui, and C. Bustamante, Science **271**(5250), 795–799 (1996).
[17] O. A. Saleh, D. B. McIntosh, P. Pincus, and N. Ribeck, Phys. Rev. Lett. **102**(6), 068301 (2009).
[18] T. Yeung, P. C. Georges, L. A. Flanagan, B. Marg, M. Ortiz, M. Funaki, N. Zahir, W. Ming, V. Weaver, and P. A. Janmey, Cell Motil. Cytoskeleton **60**(1), 24–34 (2005).
[19] Y. Aratyn-Schaus, P. W. Oakes, J. Stricker, S. P. Winter, and M. L. Gardel, J. Vis. Exp. **46**, e2173 (2010).
[20] Y. Yang, J. Lin, B. Kaytanli, O. A. Saleh, and M. T. Valentine, Soft Matter **8**, 1776–1784 (2012).
[21] F. Ziemann, J. Radler, and E. Sackmann, Biophys. J. **66**, 2210–2216 (1994).
[22] T. M. Squires and T. G. Mason, Annu. Rev. Fluid Mech. **42**(1), 413–438 (2010).
[23] C. Storm, J. J. Pastore, F. C. MacKintosh, T. C. Lubensky, and P. A. Janmey, Nature (London) **435**(7039), 191–194 (2005).
[24] J. Zhang, C. R. Daubert, and E. A. Foegeding, Rheol. Acta **44**, 622–630 (2005).
[25] T. Boudou, J. Ohayon, C. Picart, R. I. Pettigrew, and P. Tracqui, Biorheology **46**, 191–205 (2009).
[26] M. Dembo and Y.-L. Wang, Biophys. J. **76**(4), 2307–2316 (1999).
[27] S. S. Hur, Y. Zhao, Y.-S. Li, E. Botvinick, and S. Chien, Cell. Mol. Bioeng. **2**(3), 425–436 (2009).
[28] Y. L. Wang and R. J. Pelham, Methods Enzymol. **298**, 489–496 (1998).
[29] Y. Yang, J. Lin, R. Meschewski, E. Watson, and M. T. Valentine, BioTechniques **51**, 29–34 (2011).